

The CHARMM–TURBOMOLE Interface for Efficient and Accurate QM/MM Molecular Dynamics, Free Energies, and Excited State Properties

Saleh Riahi and Christopher N. Rowley*

The quantum mechanical (QM)/molecular mechanical (MM) interface between Chemistry at HARvard Molecular Mechanics (CHARMM) and TURBOMOLE is described. CHARMM provides an extensive set of simulation algorithms, like molecular dynamics (MD) and free energy perturbation, and support for mature nonpolarizable and Drude polarizable force fields. TURBOMOLE provides fast QM calculations using density functional theory or wave function methods and excited state properties. CHARMM–TURBOMOLE is well-suited for extended QM/MM MD simulations using first principles methods with large (triple- ζ) basis sets. We demonstrate these capabilities with a QM/MM simulation of $\text{Mg}^{2+}(\text{aq})$, where the MM outer

sphere water molecules are represented using the SWM4-NDP Drude polarizable force field and the ion and inner coordination sphere are represented using QM PBE, PBE0, and MP2 methods. The relative solvation free energies of Mg^{2+} and Zn^{2+} were calculated using thermodynamic integration. We also demonstrate the features for excited state properties. We calculate the time-averaged solution absorption spectrum of indole, the emission spectrum of the indole 1L_a excited state, and the electronic circular dichroism spectrum of an oxacepham. © 2014 Wiley Periodicals, Inc.

DOI: 10.1002/jcc.23716

Introduction

Among multiscale computer modeling techniques, quantum mechanical (QM)/molecular mechanical (MM) methods have the longest and most impressive histories.^[1–5] Broadly, these methods allow a relatively small but critical part of a chemical system to be represented using a QM method, while the remainder of the system is described using a MM model. As QM calculations are much more computationally demanding than MM calculations, these hybrid models are far more efficient than the equivalent pure QM model. Current QM/MM models typically have QM regions that include 10–100 atoms and MM regions that include hundreds or thousands of atoms.^[6–13]

QM/MM models can be advantageous in a variety of situations. The QM model allows a first-principles description of the critical parts of the system, so it is not necessary to parameterize a MM force field for the atoms in the QM region. They also provide a straightforward means to describe features that are difficult to represent using pure MM models, such as transition metal bonding, polarization, charge transfer, and chemical reactions. This method has been applied with considerable success to study homogeneous catalysis,^[4,14,15] solvation,^[16,17] spectroscopy,^[18,19] protein protonation states,^[20,21] and enzyme reaction mechanisms.^[6,7,22–25]

Although the efficiency of QM/MM calculations allows large systems to be modeled, these large systems often have considerable configurational variability. In particular, systems including an explicit solvent have extremely broad and complex configurational spaces. Simple techniques, like using the harmonic oscillator approximation at minimum energy structures, are no longer realistic in these cases. Instead, molecular simulation methods like molecular dynamics (MD) or Monte

Carlo must be used to sample an ensemble of configurations according to the appropriate thermodynamic distribution. This again creates a challenge, because at minimum, thousands of configurations must be sampled to generate a converged distribution. For each sequential configuration, a QM energy and gradient calculation must be performed, so the total wall-clock time of these simulations can be very long.

Commonly, these sampling issues are addressed using computationally inexpensive semiempirical QM methods like AM1^[26] or PM3.^[27] This restricts the types of systems that can be studied to those where parameters have been defined for that method. Further, approximations in these methods limit the accuracy of the computed properties. Without corrections, some popular semiempirical methods are unreliable for describing intermolecular interactions like hydrogen bonding.^[28] In recent years, density functional theory (DFT) methods emerged as an alternative; however, the computational costs of these methods are generally higher, limiting the time scale of the simulation or necessitating the use of small, less accurate basis sets. Codes using periodic plane wave basis sets have been used successfully in QM/MM simulations,^[12,29–32] although this creates another set of challenges related to basis set convergence, the use of pseudopotentials to represent core electrons, and the need for large simulation cells to avoid spurious self-interaction between the images of the periodic QM region.

S. Riahi, C. N. Rowley

Department of Chemistry, Memorial University of Newfoundland, St. John's, Newfoundland, A1B 3X7, Canada

E-mail: crowley@mun.ca

© 2014 Wiley Periodicals, Inc.

This trade off between the accuracy of the QM method and the extent of the sampling has prevented QM/MM methods from being applied when an accurate QM method and long simulation times are necessary. The proliferation of high performance computing facilities and more efficient QM methods has made it possible to perform extended QM/MM MD simulations using accurate QM methods. The goal of the CHARMM–TURBOMOLE interface is to make these simulations possible for a broader range of systems, allowing these simulations to be used more extensively in the chemical sciences. In this article, we provide an overview of the implementation and general usage of the CHARMM–TURBOMOLE QM/MM interface. We present a series of examples demonstrating the features of this code, including QM/MM MD, thermodynamic integration, and excited state features.

Why CHARMM?

While many popular molecular simulation codes have a QM/MM interface, CHARMM supports a notably broad range of QM methods. Semiempirical^[33] and tight binding DFT QM methods^[34] are integrated directly into the CHARMM source code. Quantum chemical programs Q-Chem,^[35] Gaussian 09, GAMESS–UK,^[36] and deMon^[37] are interfaced with CHARMM through a module (gukini) that executes these programs externally and parses the QM energy and gradients from their output files. Each of these QM programs provides different advantages and capabilities, providing versatility to the QM/MM features of CHARMM.

One advantage of running QM/MM simulations from within a program like CHARMM is the sophisticated molecular simulation features that are available. CHARMM provides geometry optimization, Monte Carlo, MD, replica exchange MD,^[38,39] thermostats,^[40] SHAKE constraints,^[41] and restraints. CHARMM also supports many free energy calculation methods, including free energy perturbation, thermodynamic integration, and umbrella sampling. In recent years, these methods have been used in conjunction with QM/MM methods with increasing frequency.

The CHARMM code is also attractive because of its mature support for MM force fields. The CHARMM force field is an atomistic force field that has been developed in parallel to the CHARMM simulation code.^[42] The force field includes parameters for various small molecules, liquids,^[43] proteins,^[44] carbohydrates,^[45] and nucleic acids.^[46] Beyond this conventional nonpolarizable model, the Drude polarizable force field is also supported by CHARMM.^[47] This model has been parameterized for water,^[48] ions,^[49–51] sulfur-containing compounds,^[52–54] aromatics,^[55] amides,^[56] alkanes,^[57] alcohols,^[58,59] proteins,^[60] and nucleic acids.^[61]

The use of polarizable MM models with QM/MM methods (QM/pMM) holds promise to improve the quantitative accuracy of these models because the electric field imposed on the QM region by a polarizable MM region is more realistic.^[62–66] The nonpolarizable force fields that have traditionally been used as the MM model often have inaccurate dielectric properties,^[48,67]

suggesting that polarization of the QM region induced by these models is not entirely realistic.

The Drude force field is a “charge-on-a-spring” model, where the effect of induced electron polarization is included by adding charged particles that are harmonically tethered to their parent atoms.^[47] The positions of these particles are propagated dynamically, eliminating the need for a costly self-consistent calculation of induced polarization.^[68] This is particularly attractive for QM/MM simulations because the polarizable QM/MM SCF procedure would require that the iterations simultaneously adjust the QM and MM regions.^[69] This is computationally expensive and would require substantial modifications to the QM code.

These features make CHARMM an attractive MM host program for many types of QM/MM simulations. In the instances where CHARMM is not suitable, users should consider using the ChemShell, which provides a QM/MM interface to TURBOMOLE with different functionality.^[70]

Why TURBOMOLE?

TURBOMOLE is a quantum chemical program that supports a wide range of *ab initio* methods.^[71] TURBOMOLE can perform DFT calculations using pure, hybrid, meta, metahybrid, and double hybrid exchange-correlation functionals. Dispersion corrections for most functionals are also available.^[72] Many wave function-based methods are also supported, including Hartree–Fock, second-order Møller–Plesset theory (MP2),^[73] approximate coupled cluster doubles (CC2),^[74] and coupled cluster singles and doubles (CCSD).^[75,76] As a design principle, TURBOMOLE supports a more limited set of quantum chemical methods than some other codes, but has instead focused on efficient implementations of methods with proven track records. The subprograms of TURBOMOLE used by CHARMM–TURBOMOLE support parallel execution using the Message Passing Interface (MPI) or Symmetric Multiprocessing (SMP). The full list of features of TURBOMOLE are described in a recent review.^[77]

TURBOMOLE has several advantages for performing the QM component of a QM/MM calculation. The first is a robust implementation of the resolution-of-identity (RI) approximation, which allows for efficient calculations of Coulomb integrals.^[78,79] These integrals are one of the most time consuming components of many quantum chemical calculations. In particular, the speed of DFT calculations using pure functionals can be significantly increased. Post-Hartree–Fock wave function methods like MP2 and CC2 also experience large speedups using the RI approximation in the *ricc2* module. These methods make it possible to perform QM calculations on a 10–20 atom QM region using accurate DFT or wave function methods and large basis sets (e.g., triple- ζ) and still perform relatively long MD simulations.

TURBOMOLE also has sophisticated features for the efficient calculation of excited electronic states. The *escf* module of TURBOMOLE supports the calculation of vertical excitation energies using the Tamm–Dancoff (TD) or Random Phase Approximation. The oscillator strengths and rotational

strengths are also calculated, allowing the prediction of absorption and electronic circular dichroism (ECD) spectra. The egrad subprogram calculates the gradients of excited state structures, allowing for geometry optimizations or MD simulations of excited state structures.

The CHARMM–TURBOMOLE Interface

Theory

The CHARMM–TURBOMOLE interface uses a standard QM/MM scheme, where the total potential energy (E) is the sum of the potential energies of the QM and MM regions (E_{QM} and E_{MM} , respectively), and a third term ($E_{\text{QM/MM}}$) that results from the interaction between the QM and MM regions.

$$E = E_{\text{QM}} + E_{\text{MM}} + E_{\text{QM/MM}}. \quad (1)$$

The $E_{\text{QM/MM}}$ energy is composed of terms to describe the Pauli repulsion, dispersive, and electrostatic interactions between the QM and MM regions. The Pauli repulsion and dispersion interactions are approximated by a sum of Lennard-Jones potentials between each atomic pair,

$$E_{\text{QM/MM,LJ}} = \sum_A^{N_{\text{QM}}} \sum_B^{N_{\text{MM}}} E_{\text{min,AB}} \left[\left(\frac{R_{\text{min,AB}}}{|r(A) - r(B)|} \right)^{12} - 2 \left(\frac{R_{\text{min,AB}}}{|r(A) - r(B)|} \right)^6 \right], \quad (2)$$

where E_{min} and R_{min} are the Lennard-Jones parameters for the atom pairs A and B , with A in the QM region and B in the MM region. The electrostatic interaction term is due to the Coulombic interaction between the partial charges of the MM atoms and the nuclei and electron density of the QM region. The MM–nuclear interaction is a simple pairwise Coulombic interaction for each pair of MM charges and QM nucleus. The interaction between the MM atomic point charges and QM electron density is included through one-electron integrals for each point-charge–basis-function pair in the Fock matrix,

$$F_{\text{QM/MM},\mu\nu}^{\text{elec}} = F_{\mu\nu}^{\text{QM}} - \sum_n^{\text{MM}} \left\langle \mu \left| \frac{q_n}{r_n} \right| \nu \right\rangle. \quad (3)$$

In this equation, $F_{\mu\nu}$ is the element of the Fock matrix corresponding to the basis functions μ and ν obtained from QM calculation of inner region and q_n is the charge of n th particle in the MM region. The Drude polarizable force field is integrated in exactly the same way, where the partial charge of the Drude particles interact with the QM region through one-electron integrals. This scheme allows QM/MM electrostatic interactions to be incorporated explicitly through the QM Hamiltonian without additional approximations. For example, in some other QM/MM schemes, the QM/MM electrostatic interaction is approximated by assigning partial atomic charges to the QM atoms then calculating the electrostatic energy as a sum of pairwise point-charge–point-charge interactions.^[80] Direct calculation of QM/MM electrostatics through the Fock matrix allows the QM region to be polarized by the

MM region, which is not possible in some ONIOM-type embedding methods.^[81] The drawback of this method is that there is no straightforward method to describe periodic interactions or impose distance cutoffs; CHARMM–TURBOMOLE only supports finite systems (e.g., spherical boundary conditions).

It is possible to define the QM/MM boundary across a covalent bond using the link atom approach.^[82] This is invoked in the same way as in the other CHARMM QM/MM interfaces, where the “addlink” command is executed with a selection of the pair of atoms forming the bond. A hydrogen atom along this bond vector is automatically added to the QM region in all subsequent QM/MM calculations.

Implementation

The TURBOMOLE QM/MM interface has been present in the official CHARMM source code distribution beginning with version c37b1. The current version is based on an interface to TURBOMOLE 6.5, but is generally stable across versions.

The implementation of the CHARMM–TURBOMOLE interface mirrors the GAMESS–UK and Q-Chem interfaces. The interfacing code is mostly in the *gukini* module. This module was originally developed for the GAMESS–UK interface, but has since been modified to support other QM codes. The CHARMM–TURBOMOLE interface is compiled into CHARMM when the QTURBO compilation keyword is used. Only one QM/MM interface can be incorporated into a compilation of CHARMM, so separate CHARMM executables are needed for TURBOMOLE, Q-Chem, or GAMESS calculations.

Prior to any QM/MM calculation, all the data files for a TURBOMOLE calculation (i.e., control, mos, basis, and auxbasis) must be configured by the user prior to the CHARMM–TURBOMOLE calculation. The path of these files must be specified in the “qturboinpath” environment variable. The control file of the TURBOMOLE calculation must contain the keyword “\$point_charges file = point_charges.” This keyword causes the TURBOMOLE modules to read in the point charges from the input file, which are given according to the x , y , and z positions of the charges and their magnitude in units of electrons. The TURBOMOLE options for the calculation of excited electronic states must also be configured in the control file by the user.

When a CHARMM routine requires the energy or forces of a system containing a QM region, the *gukini* module executes a Python script that is distributed with the CHARMM source code (*turbo.py*). The path of this script must be specified in the “qturboexe” environment variable. This script then executes the correct modules of TURBOMOLE. The use of this wrapper script has several advantages: the script can be modified easily to point to different installations of TURBOMOLE, change execution options, or support newer versions of TURBOMOLE. In general, the source code of CHARMM does not need to be modified and recompiled due to these modifications, simplifying its deployment.

CHARMM passes the QM nuclear coordinates and MM point charge coordinates by writing the files “coord” and

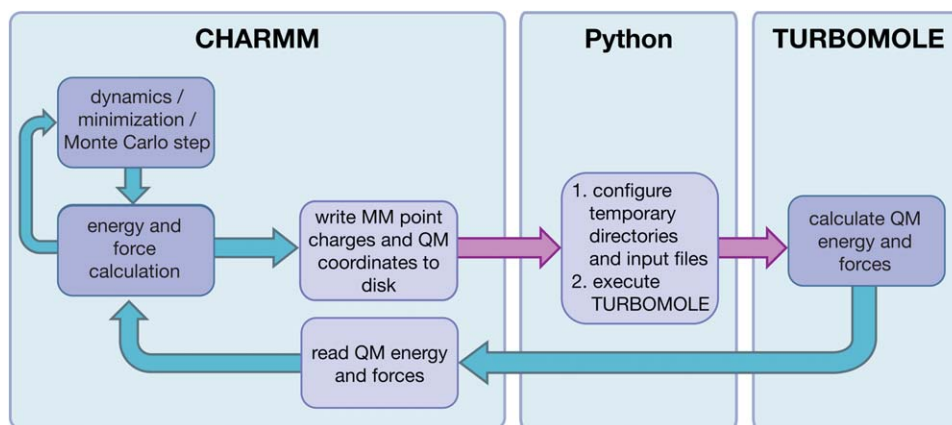


Figure 1. The program flowchart of the CHARMM–TURBOMOLE interface.

“point_charges,” respectively, to a directory reserved for data transfer between CHARMM and TURBOMOLE. The path of this directory is specified by the “qturbooutpath” environment variable. The turbo.py script copies these files to a local scratch directory with the other TURBOMOLE data files. TURBOMOLE is then executed by the turbo.py script. TURBOMOLE writes the files “gradient” and “pc_gradients,” containing the Cartesian potential energy gradients on the QM atomic centers and the MM point charges, respectively. After the TURBOMOLE calculations are complete, the “turbo.py” script copies these files to the “qturbooutpath” directory to be read by CHARMM. A schematic of this process is presented in Figure 1.

For simulations where excited state properties are calculated, the energy, oscillator strength, and rotational strength of each excitation are extracted from the TURBOMOLE output and appended to a separate log file by the turbo.py script. If other QM properties are needed (e.g., chemical shifts, partial charges, orbital energies, and so forth), the turbo.py script could be modified to store this information at each time step as well.

Photochemically active molecules can undergo spontaneous transitions between the ground and excited electronic states. Nonadiabatic MD techniques have been developed that allow “hopping” between these surfaces over the course of a MD simulation.^[83–85] Nonadiabatic dynamics is currently not implemented in CHARMM and would require substantial changes to the code. Although surface hopping is not supported, CHARMM–TURBOMOLE can be used to perform adiabatic MD on long-lived excited states, under the assumption that the molecule is unlikely to decay to the ground state in the timescale of the simulation. The egrad module of TURBOMOLE calculates the potential energy and gradients for a given electronic state. These gradients are read by CHARMM and used to propagate the dynamics of the atoms in exactly the same way that MD of the ground state are performed. When an adiabatic simulation of an excited state is being performed, the turbo.py script detects if the control file contains the “\$sexopt” keyword, indicating that gradients should be calculated for an excited state. In

this case, the egrad module is executed instead of the grad/rdgrad module.

We have also implemented support for alchemical free energy methods^[86] to determine the relative energy of two topologies. In CHARMM, the topology refers to the full set of bond, angle, and dihedral terms, atomic masses, and atom types. Alchemical methods, like free energy perturbation or thermodynamic integration, calculate the relative free energies of two different topologies. For example, to calculate the relative solvation free energies of Zn^{2+} and Mg^{2+} , we would need to define the topology for Zn^{2+} ($\lambda = 0$) and a separate topology for Mg^{2+} ($\lambda = 1$). In each energy/force evaluation, the energy and forces for both topologies must be calculated. CHARMM executes the turbo.py script with a command line argument to indicate which topology to use in the calculation. The “qturboinpath” directory must contain subdirectories named “state_0” and “state_1,” containing the TURBOMOLE data files for the $\lambda = 0$ and $\lambda = 1$ topologies, respectively. The difference in the QM electronic energy internal to these two species introduces a significant issue in these calculations, because there is no straightforward and general way to remove this effect from the computed energies. Monatomic ions are an interesting class of systems where this issue is not present, as the difference in electronic energy of the two ions in the gas phase can be subtracted separately for the calculation of the relative free energies.^[87,88]

Running a CHARMM–TURBOMOLE calculation

The configuration for a QM/MM TURBOMOLE calculation is based on a standard MM CHARMM input script. The qturboinpath, qturbooutpath, and qturboexe environment variables must be set by this script or by the shell prior to execution. The topology and coordinates of the system are defined following the normal procedure for a CHARMM calculation. If there is an existing CHARMM residue type for a molecule that is part of the QM region, it can be used directly for the QM/MM model; however, lone pair and Drude particles should be deleted. Otherwise, a new residue type for the molecule in the

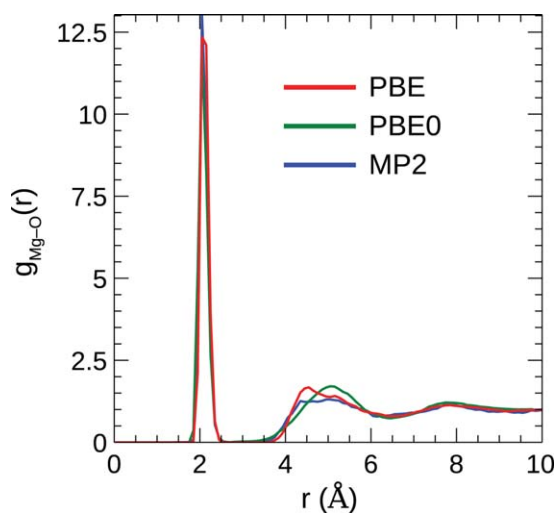


Figure 2. The radial distribution functions (rdf) calculated from the PBE, PBE0, and RI-MP2 QM/pMM MD simulations of the solvation of Mg^{2+} in water. [Color figure can be viewed in the online issue, which is available at wileyonlinelibrary.com.]

QM region must be defined in the topology/parameter files even though it will only be calculated using a QM model. It should be noted that it is not necessary to provide MM parameters for bonded terms within the QM residue like in ONIOM-type methods because these would ultimately be ignored in any case.

Lennard-Jones E_{min} and R_{min} parameters for all the atom types in the QM region must be defined in the CHARMM parameter (prm) file. The corresponding CHARMM MM Lennard-Jones parameters or those from the generalized amber force field (GAFF) are generally suitable. CHARMM determines the atomic symbols to be used in the QM calculations based on the atomic masses, so the masses defined in the topology file for these residues must correspond to those defined in the CHARMM FINDEL subroutine. The “qturbo remove select < atom selection statement > end” command deletes the MM internal energy terms for the atoms in the QM region and flags these atoms to be represented using the QM model. After this command is executed, all energy and gradient calculations will include a QM/MM calculation using TURBOMOLE.

Examples

To demonstrate the capabilities of the CHARMM–TURBOMOLE code, we present several types of QM/MM simulations. A QM/pMM simulation of $\text{Mg}^{2+}(\text{aq})$ is presented using a pure DFT functional, a hybrid DFT functional, and RI-MP2. The relative solvation free energy of Mg^{2+} and Zn^{2+} is also computed using thermodynamic integration. To demonstrate the CHARMM–TURBOMOLE features for the calculation of excited electronic states, we show the calculation of the excitation and emission spectra of aqueous indole using a QM/pMM MD simulation and the ECD spectrum of an oxacepham in acetonitrile using a QM/MM MD simulation.

DFT and MP2 QM/MM MD simulations $\text{Mg}^{2+}(\text{aq})$

An immediate application of CHARMM–TURBOMOLE is to use MD to study the configurationally averaged structure of a complex system. For sufficiently small systems (<15 atoms) it is possible to perform extended QM/MM simulations using a large, triple- ζ basis set. The use of a large basis set is important because intermolecular interactions are highly sensitive to basis set truncation and basis set superposition error.

One interesting example is $\text{Mg}^{2+}(\text{aq})$, where the ion and octahedral inner coordination sphere of water molecules can be described using QM and the rest of the system can be described using MM. While calculations using pure DFT functionals are exceptionally fast, calculations using hybrid DFT functionals (e.g., PBE0) or MP2 are also tractable. MP2 theory is an attractive method for MD simulations of liquids because intermolecular interactions calculated using MP2 are generally quite accurate if a large (e.g., triple- ζ) basis set is used.

To demonstrate these features, we performed QM/pMM MD simulations of $\text{Mg}^{2+}(\text{aq})$ using PBE,^[89] PBE0,^[90] and RI-MP2^[91–93] QM models. All simulations used the def2-TZVPP basis set^[94] for the QM region. The DFT models were simulated for 90 ps, while the MP2 model was simulated for 40 ps. The MM waters were described using the SWM4-NDP model.^[95] For comparison to a current polarizable MM force field, we also performed simulations using the Drude model for Mg^{2+} developed by Yu et al.^[51]

The Mg–O radial distribution functions (rdf) calculated from the QM/pMM simulations are presented in Figure 2. The simulations using PBE, PBE0, and MP2 QM methods show generally similar results, with a sharp peak between 2.0 and 2.1 Å corresponding to an octahedral first coordination sphere. This is in good agreement with the neutron scattering data of Bruni et al.^[96] There is slightly more variety in the diffuse second peak, where the PBE0 simulation predicts the maximum of the peak to be shifted by roughly 0.5 Å, while PBE and MP2 are in good agreement. This suggests that some differences can arise in the QM/MM interactions depending on QM model.

The wall-clock times of these simulations based on 0.1 ps QM/pMM simulations with each QM method are presented in Figure 3. The simulations using the pure DFT functional PBE are the fastest, although for this system, simulations using the hybrid PBE0 functional required only 25% more time. The simulations using RI-MP2 required took more than 500% longer than the PBE simulation, although it was still possible to complete a 40 ps RI-MP2 QM/pMM MD simulation over a 3-month period.

Relative hydration free energies of Zn^{2+} and Mg^{2+}

In this example, thermodynamic integration is used to calculate the relative hydration free energy of Zn^{2+} and Mg^{2+} . In thermodynamic integration, a coupling parameter, λ , is defined, which connects the two states such that the system is in the first state (Zn) when $\lambda = 0$ and in the second state (Mg) when $\lambda = 1$. One simple choice is to define the system as a linear combination of the two states. The potential energy of the system for any given value of λ between 0 and 1 is,

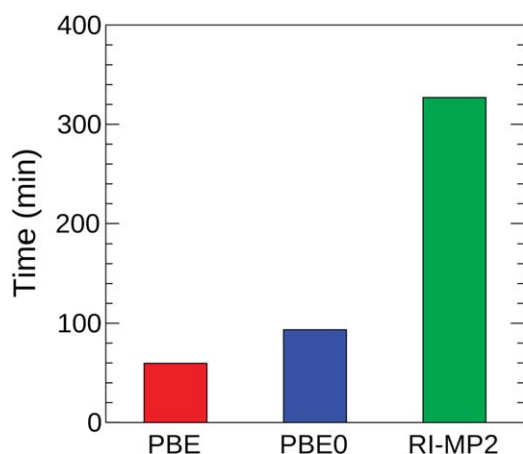


Figure 3. Wall-clock times for 0.1 ps of QM/pMM MD simulations of the system containing a Mg^{2+} ion with 6 H_2O molecules in the QM region and 445 Drude polarizable water molecules (SWM4-NDP) in the MM region, running in parallel on a 24 processor SGI C2112-4G3 compute node.

$$U_\lambda = (1 - \lambda)U_{\text{Mg}} + \lambda U_{\text{Zn}}. \quad (4)$$

Now the relative free energy of the two states can be expressed as an integral of the ensemble average of the difference in potential energy for the Mg^{2+} model and the Zn^{2+} model at the given values of λ ($\langle U_{\text{Mg}} - U_{\text{Zn}} \rangle_\lambda$),

$$\Delta A_{\text{Zn} \rightarrow \text{Mg}} = \int_{\lambda=0}^{\lambda=1} \langle U_{\text{Mg}} - U_{\text{Zn}} \rangle_\lambda d\lambda. \quad (5)$$

In practice, the relative free energy is calculated by numerically integrating the averages resulting from a series of simulations at several values of λ . The weighted histogram analysis method (WHAM)^[97] or multistate Bennett acceptance ratio^[98] method can be used instead of numerical integration.

In an earlier publication, we performed this calculation using a QM/pMM model where PBE/def2-TZVPP was used as the QM model.^[16] Here, we extend these calculations to include a PBE0/def2-TZVPP model to demonstrate the option of using hybrid functionals in CHARMM–TURBOMOLE. The difference in electronic energy of the bare cations is subtracted from the computed change in free energy.

The relative free energy of solvation of Mg^{2+} and Zn^{2+} ($\Delta A_{\text{Zn} \rightarrow \text{Mg}}$) was calculated using the Drude polarizable force field, the PBE QM/pMM model, and the PBE0 QM/pMM model. The results of these simulations are presented in Figure 4. The solvation of these two ions provides an interesting test of computational methods because the ions are effectively the same size, but Zn^{2+} has a significantly more favorable hydration free energy. This difference reflects the greater Lewis acidity of Zn^{2+} , which allows for a stronger interaction with the first coordination sphere through ligand-to-metal charge transfer.^[16] The Drude force field, which neglects charge transfer effects, significantly underestimates $\Delta A_{\text{Zn} \rightarrow \text{Mg}}$. The PBE and PBE0 QM/pMM models are both in fairly good agreement with experiment,

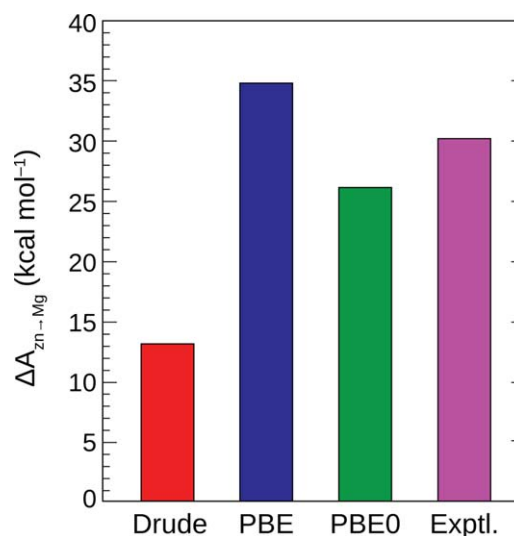


Figure 4. The relative hydration energies of Zn^{2+} and Mg^{2+} , $\Delta A_{\text{Zn} \rightarrow \text{Mg}}$, calculated using thermodynamic integration with the Drude pMM force field and QM/pMM models with PBE/def2-TZVPP and PBE0/def2-TZVPP QM models. [Color figure can be viewed in the online issue, which is available at wileyonlinelibrary.com.]

overestimating the experimental value by 4 kcal mol^{-1} in the former case but underestimating it by 3 kcal mol^{-1} in the latter. This demonstrates the sensitivity of DFT QM/MM calculations of metals to delocalization error stemming from the approximations used in the exchange-correlation functionals; “pure” functionals that do not include exact exchange tend to overestimate the stabilization that results from charge transfer^[99–101] but the PBE0 functional, which includes a 25% exact exchange component, underestimates this interaction.

Absorption and emission spectra of aqueous indole

The calculation of time-averaged electronic spectral properties from an MD simulation is a notable feature of CHARMM–TURBOMOLE. QM/MM methods provide a means to introduce the effect of the electrostatic environment into a QM model of a chromophore. The environment of a molecule has a large effect on its electronic absorption spectrum. A solvatochromic shift occurs in polar solvents that preferentially stabilize the ground or excited states of the solute, changing the wavelength of the transition between them. Likewise, chromophores in proteins will have a variety of absorption wavelengths because of different interactions with the protein.^[102] The linewidths of absorption also undergo broadening because of molecular vibrations and conformational isomerization. Linewidth broadening is generally greater in solution because of the wide variety of solvent configurations. QM/MM MD simulations have the potential to incorporate these effects in a rigorous way by calculating the electronic spectrum at each time step of a simulation, providing a time-averaged distribution of the spectral properties. In some instances, it may be more efficient to calculate the spectral properties periodically. This can be achieved through a minor modification to the turbo.py script.

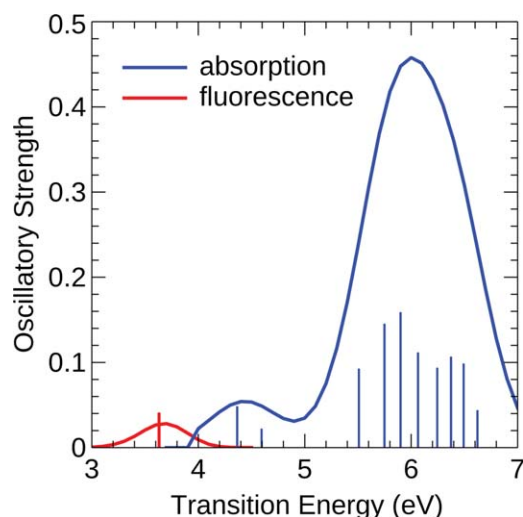
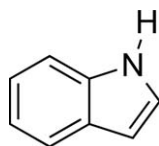


Figure 5. The absorption and emission spectra for aqueous indole calculated from QM/pMM MD simulations. The QM region was represented using PBE/def2-SVP and the MM region was represented using the SWM4-NDP Drude polarizable model. Oscillator strengths and excitation/emission energies, and excited state forces were calculated using TD-DFT. The absorption and emission spectra are calculated from 100 and 50 ps MD simulations, respectively. Vertical lines indicate the average energy and oscillator strengths of the transitions. [Color figure can be viewed in the online issue, which is available at wileyonlinelibrary.com.]

The electronic spectrum of indole is of interest as it is a common chromophore in proteins.



Indole exhibits solvatochromic shifts in both the absorption and fluorescence spectrum. The experimentally determined fluorescence lifetime of indole in water is 4.57 ns,^[103] making it an appropriate subject for an adiabatic excited state simulation. The electronic absorption spectrum of aqueous indole was calculated from a 100 ps QM/pMM simulation (Fig. 5). The emission spectrum of Figure 5 was calculated from a 50 ps adiabatic QM/pMM simulation of the 1L_a excited state. The general features and solvent effects on this spectrum are in generally good agreement with previous experimental and theoretical results.^[104,105]

The wall-clock times for 0.1 ps QM/pMM MD simulations of the electronic spectra of the ground and 1L_a excited state of aqueous indole are presented in the Figure 6. For reference, we performed a standard ground-state QM/pMM MD simulation without calculating excited state properties (labeled conventional MD). Calculating the first five excitations for the calculation of the absorption spectrum doubles the simulation time. Performing dynamics on the potential energy surface of the first excited state increases the cost of the simulation by a factor of four. Although the cost of these simulations is greater, it is still possible to perform extended MD simulations if sufficient parallel computing facilities are used for an extended period.

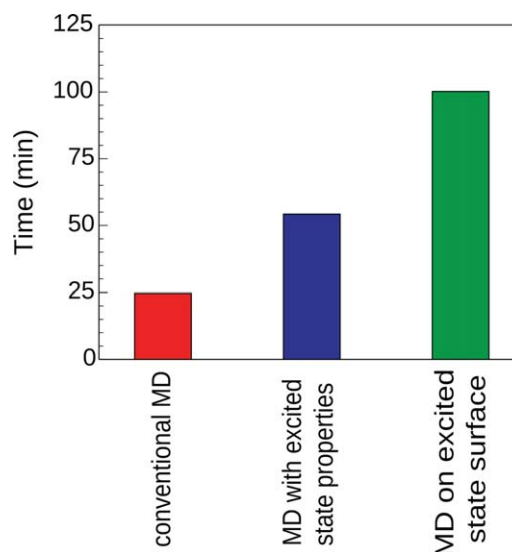
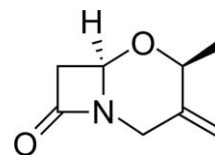


Figure 6. Wall-clock times for 0.1 ps QM/pMM MD simulations for a system containing an indole molecule represented with a PBE0/def2-SVP QM model and 445 Drude polarizable water molecules (SWM4-NDP) in the MM region, running in parallel on a 24 processor SGI C2112-4G3 compute node. [Color figure can be viewed in the online issue, which is available at wileyonlinelibrary.com.]

ECD spectrum of an oxacepham

Calculation of the electronic absorptions also provides the data that can be used to calculate the ECD spectrum of a molecule.^[106,107] This is particularly valuable for assigning the absolute stereochemistry of a chiral molecule^[108,109] or the conformation of a macromolecule.^[110,111] Again, dynamic effects can affect these spectra, especially for those in solution. The assignment of ECD spectra for flexible molecules is a challenge for methods that consider only minimum-energy structures, so the calculation of the configurationally averaged ECD spectrum from an MD simulation could be a viable strategy to help assign the absolute stereochemistry for these molecules.

To demonstrate the calculation of a configurationally averaged ECD spectrum using CHARMM-TURBOMOLE, we performed a 40 ps QM/MM MD simulation of (4S,6R)-4-methyl-3-methylene-5-oxa-1-azabicyclo[4.2.0]octan-8-one, an oxacepham antibiotic.



This molecule and a set of similar cepham antibiotics were previously examined in a combined theoretical/experimental study by Frelek et al.^[112] In the simulations presented here, the solute was represented using PBE0/def2-SV(P) and the acetonitrile solvent was represented using a six-site MM model. Four singlet excitations were calculated using TD-DFT at each time step.

The calculated ECD spectrum of the oxacepham calculated from the QM/MM MD simulation is presented in Figure 7. For comparison, the spectrum calculated using only the minimum-energy structure with a continuum solvent model is also

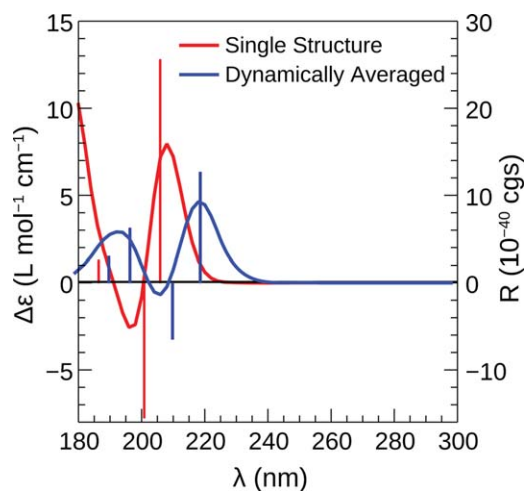


Figure 7. The calculated electronic circular dichroism (ECD) spectrum of an oxacepham in a sphere of 215 acetonitrile molecules and optimized structure in continuum solvent model (COSMO model with $\epsilon = 37.5$). Vertical lines indicate the average rotational strength and absorption wavelength of the contributing transitions. The dynamically averaged spectrum was calculated from a 40 ps of QM/MM simulation using a PBE0/SV(P) QM model in an explicit MM acetonitrile solvent. [Color figure can be viewed in the online issue, which is available at wileyonlinelibrary.com.]

shown. The large differences between the two spectra reflect that both the excitation energy and rotational strength of electronic absorptions have large distributions in flexible molecules. This is illustrated in Figure 8, which shows the distribution of the rotational strength and excitation energies of the second excitation sampled in the QM/MM MD simulation. The wavelength of the absorption has a 20 nm range and a rotational strength in the -25×10^{-40} – 20×10^{-40} cgs range. Significantly, the values of the minimum energy structure do not coincide with the most probable values of the distribution. The ability of QM/MM MD simulations to sample the configurational freedom of flexible molecules in an explicit solvent, and the corresponding variety in absorption energies and rotational strengths, may allow the absolute stereochemistry of flexible chiral molecules to be determined more reliably using ECD.

Computational Details

All the QM/MM MD simulations were performed on the Mammouth-Parallel II facility of Compute Canada. The computational timings reported are determined from simulations performed on SGI C2112-4G3 compute nodes. These nodes contain dual AMD Opteron 6172 12-core processors with 2.1 GHz clock speeds. All simulations were performed on one dedicated node (24 processors in parallel).

Simulations of $\text{Mg}^{2+}(\text{aq})$ and $\text{Zn}^{2+}(\text{aq})$

The simulations of Mg^{2+} and Zn^{2+} hydration were performed using a water sphere of 14 Å radius, composed of 445 water molecules represented using the SWM4-NDP Drude polarizable force field. The water molecules were restrained in the sphere using a half-harmonic spherical boundary potential with a force constant of $2 \text{ kcal mol}^{-1} \text{ Å}^{-2}$. The QM region was com-

posed of the ion and an inner coordination sphere of six water molecules. The ions were restrained to the center of sphere with a harmonic potential with the force constant of $5 \text{ kcal mol}^{-1} \text{ Å}^{-2}$. The nonbonded cutoff and pairing list distances were set such that all Lennard-Jones and Coulombic interactions were included in full. The system was coupled to a dual Langevin thermostat, where the atomic centers were coupled to a thermostat with a temperature of 298 K and a friction coefficient of 5 ps^{-1} and the Drude particles were coupled to a thermostat with a temperature of 1 K and a friction coefficient of 10 ps^{-1} .

The QM/pMM simulations of the Mg^{2+} system were performed using PBE, PBE0, and RI-MP2 using the def2-TZVPP basis set method for the QM region. A 1-fs (10^{-15} s) time step was used in all simulations. For the extended MD simulations of Mg^{2+} using PBE and PBE0, the system was equilibrated for 30 ps prior to a 90 ps production simulation. The QM/pMM MD simulation using the RI-MP2/def2-TZVPP QM model was 40 ps long. A 10^{-7} Hartree energy convergence criteria and a 10^{-7} density matrix convergence criteria was used in the SCF calculation. The m5 grid was used to calculate the exchange-correlation energy in the DFT calculations to minimize numerical error in the energy and gradient calculations that could introduce significant issues with energy conservation into the simulations.

In the thermodynamic integration calculation of the relative hydration free energy ($\Delta A_{\text{Zn-Mg}}$), 11 simulations were performed at values of λ between 0 and 1 ($\lambda = 0.0, 0.1, 0.2, 0.3, 0.4, 0.5, 0.6, 0.7, 0.8, 0.9$, and 1.0). For each value of λ , a 15 ps simulation was performed to equilibrate the system and a 50 ps simulation was performed to determine averages of $\langle U_{\text{Zn}} - U_{\text{Mg}} \rangle_{\lambda}$. The WHAM^[97] was used to calculate the relative free energy.

Electronic spectrum of aqueous indole

The simulations of aqueous indole used the same water sphere, boundary conditions, and nonbonded interaction

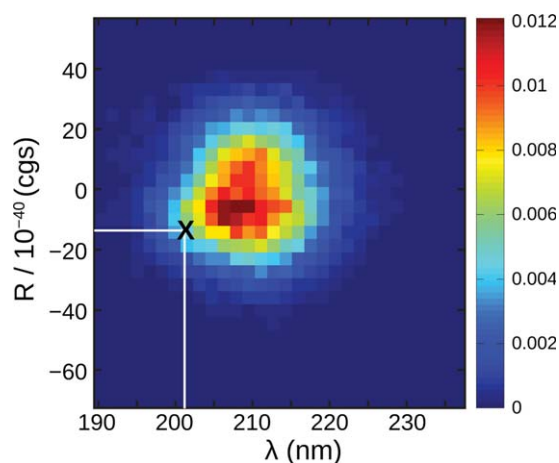


Figure 8. The distribution of the rotational strength, R , for the second transition of the ECD spectrum. The rotational strength and absorption wavelength of this transition in the minimum geometry structure is indicated by the black X ($R = -15.5 \times 10^{-40} \text{ cgs}$, $\lambda = 201 \text{ nm}$). [Color figure can be viewed in the online issue, which is available at wileyonlinelibrary.com.]

settings that were used in the Mg^{2+} simulations. One indole molecule was inserted in the center of sphere. This molecule was restrained to remain at the center of this sphere by a harmonic potential applied to its center of mass with the force constant of $5 \text{ kcal mol}^{-1} \text{ \AA}^{-2}$. The initial configuration was generated from a 1-ns MD simulation using the Drude polarizable force field for indole developed Lopes et al.^[113] In the QM/pMM simulation, the indole molecule was represented using PBE0/def-SVP^[114] and the water molecules were represented using the SWM4-NDP model. The Lennard-Jones parameters from the Drude model of indole were used for the nonbonded QM/MM interactions between indole and the solvent. A 70-ps QM/pMM MD simulation was performed to equilibrate the system, followed by a 100-ps-production MD simulation. These simulations used the same time step, nonbonded interaction, and thermostat settings as the $\text{Mg}^{2+}(\text{aq})$ system. In the production simulation, the excitation energy and oscillator strengths of the first 10 excited electronic states were calculated and recorded at each time step.

The adiabatic MD simulation of the 1L_a excited state was performed using the same system and settings as the simulation of the ground state. A 40-ps QM/pMM MD simulation was performed to equilibrate the system. A 50-ps QM/pMM MD simulation was performed to sample the distributions for the excited state emission spectrum. The egrad module of TURBOMOLE was used to calculate the energy and forces for the first excited electronic state.

The absorption and emission spectra in Figure 5 were calculated using a line width of $\sigma=0.4 \text{ eV}$ for each transition using the equation,

$$F(\omega) = \sum_i^{\text{peaks}} \frac{1}{T} \sum_t^T \frac{1}{\sigma \sqrt{\pi}} e^{-\left(\frac{\omega - \omega_i^t}{\sigma}\right)^2} f_i^t. \quad (6)$$

In this equation, the first sum is over the transition number and second sum is over the time series generated by the MD simulation. ω_i^t and f_i^t are the transition energy and oscillator strength corresponding to the i th electronic transition at time t . T is the number of time steps in the trajectory.

ECD spectrum

The ECD calculations were performed using a 15-Å sphere containing 219 acetonitrile molecules with the same boundary conditions and nonbonded settings was used in aqueous systems. The solute was represented using the PBE0/SV(P) QM model and the acetonitrile molecules were represented with the nonpolarizable all-atom model developed by Lyubartsev and Nikitin.^[115] In this demonstration, we calculate the ECD spectrum of the oxacepham (4S,6R)-4-methyl-3-methylene-5-oxa-1-azabicyclo[4.2.0]octan-8-one. The molecule was placed at the center of the sphere. The Lennard-Jones parameters for the oxacepham molecule were obtained from GAFF force field parameters using ANTECHAMBER module.^[116,117] A 5-ps QM/MM MD simulation was performed to equilibrate the system. A 40-ps QM/MM MD simulation was performed to sample the distribution of ECD transition energies and rotational

strengths. The four lowest energy electronic transitions were calculated at each time step. The ECD spectrum in Figure 7 was calculated with the equation,

$$\Delta(\lambda) = \frac{1}{2.297 \times 10^{-39} \sqrt{\pi} \sigma} \sum_i^{\text{peaks}} \frac{1}{T} \sum_t^T e^{-\left(\frac{\lambda - \lambda_i^t}{\sigma}\right)^2} \lambda_i^t R_i^t, \quad (7)$$

where λ_i^t and R_i^t are the transition energy and rotational strength (in cgs units, $10^{-40} \text{ erg cm}^3$) corresponding to the transition i , at time t . A linewidth of $\sigma=0.1 \text{ nm}$ was used for each transition.

Conclusions

A QM/MM interface with TURBOMOLE has been incorporated into CHARMM as of version c37b1. Using this code, a QM model in TURBOMOLE can be combined with a nonpolarizable or Drude polarizable force field model in CHARMM to perform QM/MM MD simulations with significant time scales (100 ps). QM/MM MD simulations using DFT and MP2 QM models with triple- ζ basis sets for the QM region and the SWM4-NDP MM model for the MM region were demonstrated in a simulation of $\text{Mg}^{2+}(\text{aq})$. The simulations using a pure DFT functional are most efficient. The simulation using the hybrid PBE0 functional was roughly 1.3 times more computationally expensive than the one using the pure PBE functional. Simulations using RI-MP2 were 4.4 times more expensive than those using a pure DFT functional. The calculated radial distribution functions in this instance were in good agreement with each other and experimental $\text{Mg}^{2+} - \text{O}$ distances.

The relative solvation free energy of Mg^{2+} and Zn^{2+} was calculated using the Drude polarizable force field and QM/pMM simulations with the PBE and PBE0 functionals. The free energies were calculated using thermodynamic integration via a dual topology formalism. In each case, the calculated free energy was in agreement with the experimental value within 5 kcal mol^{-1} .

A feature allowing the calculation of electronic-excited state properties was also demonstrated. The excitation spectrum of indole in an explicit water solvent was calculated by calculating TD-DFT excitation energies and oscillator strengths each configuration of a MD simulation. These data were combined to generate the ensemble-averaged spectrum. The ensemble-averaged emission spectrum of the long-lived 1L_a excited state of indole was calculated from an adiabatic QM/pMM simulation. Lastly, the time-averaged ECD spectrum was calculated from a QM/MM simulation of an oxacepham in a nonpolarizable acetonitrile solvent. These methods are widely applicable to include the effects of solute vibrations, conformational isomerization, and solvation.

Acknowledgments

The authors would like to thank the Memorial University of Newfoundland, NSERC of Canada for funding through a Discovery Grant (Application No. 418505-2012), and the Research and Development Corporation of Newfoundland for an Ignite R&D grant. Computational resources were provided by the Calcul Quebec consortium of

Compute Canada (Project ID: djc-615-ac). The authors thank Tiffany Tozer for a thorough reading of the manuscript.

Keywords: quantum mechanical/molecular mechanical-CHARMM · TURBOMOLE · ion solvation · electronic absorption spectrum · emission spectrum · electronic circular dichroism spectrum · polarizable force field

How to cite this article: S. Riahi, C. N. Rowley. *J. Comput. Chem.* **2014**, 35, 2076–2086. DOI: 10.1002/jcc.23716

- [1] P. D. Lyne, M. Hodoscek, M. Karplus, *J. Phys. Chem. A* **1999**, 103, 3462.
- [2] H. M. Senn, W. Thiel, *Angew. Chem. Int. Ed.* **2009**, 48, 1198.
- [3] R. A. Friesner, V. Guallar, *Annu. Rev. Phys. Chem.* **2005**, 56, 389.
- [4] T. K. Woo, L. Cavallo, T. Ziegler, *Theor. Chem. Acc.* **1998**, 100, 307.
- [5] T. K. Woo, P. M. Margl, P. E. Blöchl, T. Ziegler, *J. Phys. Chem. B* **1997**, 101, 7877.
- [6] P. Hu, S. Wang, Y. Zhang, *J. Am. Chem. Soc.* **2008**, 130, 3806.
- [7] P. Hu, Y. Zhang, *J. Am. Chem. Soc.* **2006**, 128, 1272.
- [8] Y. Shi, Y. Zhou, S. Wang, Y. Zhang, *J. Phys. Chem. Lett.* **2013**, 4, 491.
- [9] G. S. Sirin, Y. Zhou, L. Lior-Hoffmann, S. Wang, Y. Zhang, *J. Phys. Chem. B* **2012**, 116, 12199.
- [10] L. R. Rutledge, S. D. Wetmore, *J. Am. Chem. Soc.* **2011**, 133, 16258.
- [11] H. Gómez, I. Polyak, W. Thiel, J. M. Lluch, L. Masgrau, *J. Am. Chem. Soc.* **2012**, 134, 4743.
- [12] J. Garrec, C. Patel, U. Rothlisberger, E. Dumont, *J. Am. Chem. Soc.* **2012**, 134, 2111.
- [13] C. A. MacDonald, E. A. C. Bushnell, J. W. Gauld, R. J. Boyd, *Phys. Chem. Chem. Phys.* **2014**, 16, 16284.
- [14] C. N. Rowley, T. K. Woo, *Organometallics* **2011**, 30, 2071.
- [15] T. Woo, P. Margl, L. Deng, L. Cavallo, T. Ziegler, *Catal. Today* **1999**, 50, 479.
- [16] S. Riahi, B. Roux, C. N. Rowley, *Can. J. Chem.* **2013**, 91, 552.
- [17] M. Peschke, A. T. Blades, P. Kebarle, *J. Am. Chem. Soc.* **2000**, 122, 10440.
- [18] S. Sinnecker, F. Neese, *J. Comput. Chem.* **2006**, 27, 1463.
- [19] M. Nonella, G. Mathias, P. Tavan, *J. Phys. Chem. A* **2003**, 107, 8638.
- [20] P. Goyal, J. Lu, S. Yang, M. R. Gunner, Q. Cui, *Proc. Natl. Acad. Sci. USA* **2013**, 110, 18886.
- [21] H. Yu, T. M. Griffiths, *Phys. Chem. Chem. Phys.* **2014**, 16, 5785.
- [22] S. Shaik, S. Cohen, Y. Wang, H. Chen, D. Kumar, W. Thiel, *Chem. Rev.* **2010**, 110, 949.
- [23] F. Claeysens, J. N. Harvey, F. R. Manby, R. A. Mata, A. J. Mulholland, K. E. Ranaghan, M. Schütz, S. Thiel, W. Thiel, H.-J. Werner, *Angew. Chem. Int. Ed.* **2006**, 45, 6856.
- [24] E. Rosta, W. Yang, G. Hummer, *J. Am. Chem. Soc.* **2014**, 136, 3137.
- [25] E. Rosta, M. Nowotny, W. Yang, G. Hummer, *J. Am. Chem. Soc.* **2011**, 133, 8934.
- [26] M. J. S. Dewar, W. Thiel, *J. Am. Chem. Soc.* **1977**, 99, 4899.
- [27] J. J. P. Stewart, *J. Comput. Chem.* **1989**, 10, 209.
- [28] J. Řezáč, P. Hobza, *J. Chem. Theory Comput.* **2012**, 8, 141.
- [29] A. Laio, J. VandeVondele, U. Rothlisberger, *J. Chem. Phys.* **2002**, 116, 6941.
- [30] T. Laino, F. Mohamed, A. Laio, M. Parrinello, *J. Chem. Theory Comput.* **2005**, 1, 1176.
- [31] T. Laino, F. Mohamed, A. Laio, M. Parrinello, *J. Chem. Theory Comput.* **2006**, 2, 1370.
- [32] S. Wang, E. A. Orabi, S. Baday, S. Bernèche, G. Lamoureux, *J. Am. Chem. Soc.* **2012**, 134, 10419.
- [33] M. J. Field, P. A. Bash, M. Karplus, *J. Comput. Chem.* **1990**, 11, 700.
- [34] Q. Cui, M. Elstner, E. Kaxiras, T. Frauenheim, M. Karplus, *J. Phys. Chem. B* **2001**, 105, 569.
- [35] H. L. Woodcock, M. Hodošček, A. T. B. Gilbert, P. M. W. Gill, H. F. Schaefer, B. R. Brooks, *J. Comput. Chem.* **2007**, 28, 1485.
- [36] K. P. Eurenium, D. C. Chatfield, B. R. Brooks, M. Hodoscek, *Int. J. Quantum Chem.* **1996**, 60, 1189.
- [37] B. Lev, R. Zhang, A. de la Lande, D. Salahub, S. Y. Noskov, *J. Comput. Chem.* **2010**, 31, 1015.
- [38] D. J. Earl, M. W. Deem, *Phys. Chem. Chem. Phys.* **2005**, 7, 3910.
- [39] W. Jiang, M. Hodoscek, B. Roux, *J. Chem. Theory Comput.* **2009**, 5, 2583.
- [40] W. G. Hoover, *Phys. Rev. A* **1985**, 31, 1695.
- [41] W. van Gunsteren, H. Berendsen, *Mol. Phys.* **1977**, 34, 1311.
- [42] X. Zhu, P. E. M. Lopes, A. D. MacKerell, *WIREs Comput. Mol. Sci.* **2012**, 2, 167.
- [43] J. B. Klauda, R. M. Venable, J. A. Freites, J. W. O'Connor, D. J. Tobias, C. Mondragon-Ramirez, I. Vorobyov, A. D. MacKerell, R. W. Pastor, *J. Phys. Chem. B* **2010**, 114, 7830.
- [44] J. Huang, A. D. MacKerell, *J. Comput. Chem.* **2013**, 34, 2135.
- [45] O. Guvench, S. S. Mallajosyula, E. P. Raman, E. Hatcher, K. Vanommeslaeghe, T. J. Foster, F. W. Jamison, A. D. MacKerell, *J. Chem. Theory Comput.* **2011**, 7, 3162.
- [46] K. Hart, N. Foloppe, C. M. Baker, E. J. Denning, L. Nilsson, A. D. MacKerell, *J. Chem. Theory Comput.* **2012**, 8, 348.
- [47] P. Lopes, B. Roux, A. D. MacKerell, *Theor. Chim. Acta* **2009**, 124, 11.
- [48] G. Lamoureux, A. D. MacKerell, B. Roux, *J. Chem. Phys.* **2003**, 119, 5185.
- [49] G. Lamoureux, B. Roux, *J. Phys. Chem. B* **2006**, 110, 3308.
- [50] T. W. Whitfield, S. Varma, E. Harder, G. Lamoureux, S. B. Rempe, B. Roux, *J. Chem. Theory Comput.* **2007**, 3, 2068.
- [51] H. Yu, T. W. Whitfield, E. Harder, G. Lamoureux, I. Vorobyov, V. M. Anisimov, A. D. MacKerell, B. Roux, *J. Chem. Theory Comput.* **2010**, 6, 774.
- [52] S. Riahi, C. N. Rowley, *J. Phys. Chem. B* **2013**, 117, 5222.
- [53] S. Riahi, C. N. Rowley, *J. Phys. Chem. B* **2014**, 118, 1373.
- [54] X. Zhu, A. D. MacKerell, *J. Comput. Chem.* **2010**, 31, 2330.
- [55] P. E. M. Lopes, G. Lamoureux, B. Roux, A. D. MacKerell, *J. Phys. Chem. B* **2007**, 111, 2873.
- [56] E. Harder, V. M. Anisimov, T. Whitfield, A. D. MacKerell, B. Roux, *J. Phys. Chem. B* **2008**, 112, 3509.
- [57] I. V. Vorobyov, V. M. Anisimov, A. D. MacKerell, *J. Phys. Chem. B* **2005**, 109, 18988.
- [58] X. He, P. E. M. Lopes, A. D. MacKerell, *Biopolymers* **2013**, 99, 724.
- [59] V. M. Anisimov, I. V. Vorobyov, B. Roux, A. D. MacKerell, *J. Chem. Theory Comput.* **2007**, 3, 1927.
- [60] P. E. M. Lopes, J. Huang, J. Shim, Y. Luo, H. Li, B. Roux, A. D. MacKerell, *J. Chem. Theory Comput.* **2013**, 9, 5430.
- [61] A. Savelyev, A. D. MacKerell, *J. Comput. Chem.* **2014**, 35, 1219.
- [62] D. P. Geerke, S. Thiel, W. F. van Gunsteren, *J. Chem. Theory Comput.* **2007**, 3, 1499.
- [63] E. Boulanger, W. Thiel, *J. Chem. Theory Comput.* **2012**, 8, 4527.
- [64] E. Boulanger, W. Thiel, *J. Chem. Theory Comput.* **2014**, 10, 1795.
- [65] Z. Lu, Y. Zhang, *J. Chem. Theory Comput.* **2008**, 4, 1237.
- [66] C. N. Rowley, B. Roux, *J. Chem. Theory Comput.* **2012**, 8, 3526.
- [67] C. Coleman, P. J. van Maaren, M. Hong, J. S. Hub, L. T. Costa, D. van der Spoel, *J. Chem. Theory Comput.* **2012**, 8, 61.
- [68] G. Lamoureux, B. Roux, *J. Chem. Phys.* **2003**, 119, 3025.
- [69] D. Bakowies, W. Thiel, *J. Phys. Chem.* **1996**, 100, 10580.
- [70] S. Metz, J. Kästner, A. A. Sokol, T. W. Keal, P. Sherwood, *WIREs Comput. Mol. Sci.* **2014**, 4, 101.
- [71] TURBOMOLE V6.5 **2013**, a development of University of Karlsruhe and Forschungszentrum Karlsruhe GmbH, 1989–2007, TURBOMOLE GmbH, since 2007. Available at: <http://www.turbomole.com>. Accessed on August 27, 2014.
- [72] S. Grimme, J. Antony, S. Ehrlich, H. Krieg, *J. Chem. Phys.* **2010**, 132, 154104.
- [73] C. Möller, M. S. Plesset, *Phys. Rev.* **1934**, 46, 618.
- [74] O. Christiansen, H. Koch, P. Jørgensen, *Chem. Phys. Lett.* **1995**, 243, 409.
- [75] J. Čížek, On the Use of the Cluster Expansion and the Technique of Diagrams in Calculations of Correlation Effects in Atoms and Molecules; Wiley, **2007**, pp. 35–89.
- [76] G. D. Purvis, R. J. Bartlett, *J. Chem. Phys.* **1982**, 76, 1910.
- [77] F. Furche, R. Ahlrichs, C. Hättig, W. Klopper, M. Sierka, F. Weigend, *WIREs Comput. Mol. Sci.* **2014**, 4, 91.
- [78] K. Eichkorn, O. Treutler, H. Öhm, M. Häser, R. Ahlrichs, *Chem. Phys. Lett.* **1995**, 240, 283.

- [79] K. Eichkorn, F. Weigend, O. Treutler, R. Ahlrichs, *Theor. Chem. Acc.* **1997**, 97, 119.
- [80] R. C. Walker, M. F. Crowley, D. A. Case, *J. Comput. Chem.* **2008**, 29, 1019.
- [81] L. W. Chung, H. Hirao, X. Li, K. Morokuma, *WIREs Comput. Mol. Sci.* **2012**, 2, 327.
- [82] U. C. Singh, P. A. Kollman, *J. Comput. Chem.* **1986**, 7, 718.
- [83] J. C. Tully, R. K. Preston, *J. Chem. Phys.* **1971**, 55, 562.
- [84] E. Tapavicza, I. Tavernelli, U. Rothlisberger, *Phys. Rev. Lett.* **2007**, 98, 023001.
- [85] E. Tapavicza, G. D. Bellchambers, J. C. Vincent, F. Furche, *Phys. Chem. Chem. Phys.* **2013**, 15, 18336.
- [86] C. Chipot, A. Pohorille, Eds., *Free Energy Calculations: Theory and Applications in Chemistry and Biology*, Vol. 86; Springer Series in Chemical Physics; Springer, Berlin, **2007**.
- [87] R. Zhang, B. Lev, J. E. Cuervo, S. Y. Noskov, D. R. Salahub, In *Combining Quantum Mechanics and Molecular Mechanics. Some Recent Progresses in QM/MM Methods*, Vol. 59; Advances in Quantum Chemistry; J. R. Sabin, E. Brändas, Eds.; Academic Press, **2010**, pp. 353–400.
- [88] B. Lev, B. Roux, S. Y. Noskov, *J. Chem. Theory Comput.* **2013**, 9, 4165.
- [89] J. P. Perdew, K. Burke, M. Ernzerhof, *Phys. Rev. Lett.* **1996**, 77, 3865.
- [90] C. Adamo, V. Barone, *J. Chem. Phys.* **1999**, 110, 6158.
- [91] F. Weigend, M. Häser, *Theor. Chem. Acc.* **1997**, 97, 331.
- [92] F. Weigend, M. Häser, H. Patzelt, R. Ahlrichs, *Chem. Phys. Lett.* **1998**, 294, 143.
- [93] A. Hellweg, C. Hättig, S. Höfener, W. Klopper, *Theor. Chem. Acc.* **2007**, 117, 587.
- [94] F. Weigend, R. Ahlrichs, *Phys. Chem. Chem. Phys.* **2005**, 7, 3297.
- [95] G. Lamoureux, E. Harder, I. V. Vorobyov, B. Roux, A. D. MacKerell, *Chem. Phys. Lett.* **2006**, 418, 245.
- [96] F. Bruni, S. Imberti, R. Mancinelli, M. A. Ricci, *J. Chem. Phys.* **2012**, 136, 064520.
- [97] S. Kumar, J. M. Rosenberg, D. Bouzida, R. H. Swendsen, P. A. Kollman, *J. Comput. Chem.* **1992**, 13, 1011.
- [98] M. R. Shirts, J. D. Chodera, *J. Chem. Phys.* **2008**, 129, 124105.
- [99] A. J. Cohen, P. Mori-Sánchez, W. Yang, *Science* **2008**, 321, 792.
- [100] J. M. Smith, Y. Jami Alahmadi, C. N. Rowley, *J. Chem. Theory Comput.* **2013**, 9, 4860.
- [101] E. R. Johnson, A. Otero-de-la Roza, S. G. Dale, *J. Chem. Phys.* **2013**, 139, 184116.
- [102] M. Neri, S. Vanni, I. Tavernelli, U. Rothlisberger, *Biochemistry* **2010**, 49, 4827.
- [103] M. Vincent, J. Gallay, A. P. Demchenko, *J. Phys. Chem.* **1995**, 99, 14931.
- [104] H. Lami, *J. Chem. Phys.* **1977**, 67, 3274.
- [105] M. Wohlgemuth, V. Bonaïć-Koutecký, R. Mitrić, *J. Chem. Phys.* **2011**, 135, 054105.
- [106] T. D. Crawford, M. C. Tam, M. L. Abrams, *J. Phys. Chem. A* **2007**, 111, 12057.
- [107] I. Warnke, F. Furche, *WIREs Comput. Mol. Sci.* **2012**, 2, 150.
- [108] N. Berova, L. D. Bari, G. Pescitelli, *Chem. Soc. Rev.* **2007**, 36, 914.
- [109] E. Giorgio, K. Tanaka, L. Verotta, K. Nakanishi, N. Berova, C. Rosini, *Chirality* **2007**, 19, 434.
- [110] Z. Brkljača, K. Condić-Jurkić, A.-S. Smith, D. M. Smith, *J. Chem. Theory Comput.* **2012**, 8, 1694.
- [111] Z. Brkljača, M. Mališ, D. M. Smith, A.-S. Smith, *J. Chem. Theory Comput.* **2014**, 10, 3270.
- [112] J. Frelek, P. Kowalska, M. Masnyk, A. Kazimierski, A. Korda, M. Woźnica, M. Chmielewski, F. Furche, *Chem. Eur. J.* **2007**, 13, 6732.
- [113] P. E. M. Lopes, G. Lamoureux, A. D. MacKerell, *J. Comput. Chem.* **2009**, 30, 1821.
- [114] D. Rappoport, F. Furche, *J. Chem. Phys.* **2005**, 122, 064105.
- [115] A. M. Nikitin, A. P. Lyubartsev, *J. Comput. Chem.* **2007**, 28, 2020.
- [116] J. Wang, W. Wang, P. A. Kollman, D. A. Case, *J. Mol. Graph. Modell.* **2006**, 25, 247.
- [117] J. Wang, R. M. Wolf, J. W. Caldwell, P. A. Kollman, D. A. Case, *J. Comput. Chem.* **2004**, 25, 1157.

Received: 19 July 2014

Revised: 4 August 2014

Accepted: 7 August 2014

Published online on 1 September 2014